Interfacial thermal conductance in multilayer graphene/phosphorene heterostructure

Ying-Yan Zhang [1], Qing-Xiang Pei [2], Yiu-Wing Mai [3] and Siu-Kai Lai [4]

[1] *School of Computing, Engineering and Mathematics, Western Sydney University, Penrith, NSW 2751, Australia.*

[2] *Institute of High Performance Computing, A*STAR, Singapore 138632, Singapore.*

[3] *Centre for Advanced Materials Technology, School of Aerospace, Mechanical and Mechatronic Engineering, The University of Sydney, Sydney, NSW 2006, Australia*

[4] *Department of Civil and Environmental Engineering, The Hong Kong Polytechnic University, Hung Hom, Kowloon, Hong Kong, China*

E-mail: *yingyan.zhang@westernsydney.edu.au* and *peiqx@ihpc.a-star.edu.sg*

Abstract

Vertical integration of two-dimensional materials has recently appeared as an effective method for the design of novel nano-scale devices. Using non-equilibrium molecular dynamics simulations, we study the interfacial thermal transport property of graphene/phosphorene heterostructures where phosphorene is sandwiched in between graphene. Various modulation techniques are thoroughly explored. We found that the interfacial thermal conductance at the interface of graphene and phosphorene can be enhanced significantly by using vacancy defects, hydrogenation and cross-plane compressive strain. By contrast, reduction in the interfacial thermal conductance can be achieved by using cross-plane tensile strain. Our results provide important guidelines for manipulating the thermal transport in graphene/phosphorene based-nano-devices.

Keywords: Interfacial thermal conductance; graphene/phosphorene heterostructures; molecular dynamics simulations; defects; strain.

1. Introduction

In recent years, two-dimensional (2D) materials have become one of the hottest research areas owing to the discovery of graphene [1]. Graphene is the first isolated 2D material with a hexagonal lattice of sp^2 hybridized carbon atoms. It is the strongest material with the highest thermal conductivity and fastest electron mobility among all materials known in the world [2]. The only shortcoming of graphene is its zero band-gap which limits its practical applications in electronic devices [3]. The discovery of graphene has also advanced the development of other 2D materials, such as silicene and the transition metal dichalchogenides. Very recently, phosphorene, single layer black phosphorus (BP) arranged in a puckered lattice, was isolated from the bulk BP structures [4, 5]. Theoretical and experimental studies [4-8] have revealed that phosphorene is an anisotropic 2D semiconductor with high carrier mobility and a large direct band gap of ~1.5 eV, making it promising for many potential applications in nano-electronics, such as field-effect transistors and photo-transistors. Phosphorene is also found to have interesting thermal properties [9, 10] and a high figure of merit (ZT value) at room temperature [11].

Currently, vertical van der Waals (vdW) heterostructures based on 2D materials are being considered as a novel way to engineer materials for device applications [12]. A heterostructured composite comprises two or more different materials assembled in a layer-to-layer format via non-bonded vdW interactions between the layers. These non-bonded vdW interactions ensure the integrity of different materials and preserve their individual properties. Graphene has been used widely to form different heterostructures [13-20] e.g., graphene/MoS_2 (molybdenum disulfide) and graphene/h-BN (hexagonal boron nitride). Most recently, a new heterostructure based on graphene and phosphorene is proposed. By means of density functional theory calculations, Padilha *et al*. [21] investigated the structural and electronic properties of single-layer and bi-layer phosphorene with graphene. They showed

that both the properties of graphene and phosphorene are well preserved upon contact. Also, it is possible to tune the position of the band structures of phosphorene relative to that of graphene through the application of an external electric field perpendicular to the system. Chen *et al*. [22] fabricated a stable sandwiched heterostructure by encapsulating atomically thin BP between h-BN layers. They found that this heterostructure has an ultra-clean interface which allows high field-effect mobility at room temperature and high on-off ratios. BP sandwiched in h-BN layers remains intact and preserves high quality under ambient conditions.

The thermal properties of 2D materials and their heterostructures are very important for efficient heat dissipation in nano-electronic devices based on 2D materials. Based on available studies [13-24], it is evident that the incompatibility of the two different materials normally poses a strong resistance to the heat transport at the interface and is hence a major obstacle for effective heat dissipation. In this paper, we investigate the interfacial thermal transport properties of the graphene/phosphorene heterostructure by using molecular dynamics (MD) simulations, hitherto not reported. Various factors, including vacancy defects, hydrogenation, external strain and interfacial interaction strength are closely examined.

2. Model and simulation method

The simulation model of a heterostructure with 16-layer phosphorene sandwiched in 8-layer graphene is shown in Fig. 1. The in-plane is along x and y directions while the cross-plane is along z-direction. The square in-plane has a side length of about 2.6 nm while the size in the cross-plane direction is about 14 nm. Periodic boundary conditions are applied in all three directions. All the MD simulations are carried out by using the large-scale atomic/molecular massively parallel simulator (LAMMPS) package [25]. The Stillinger-Weber (SW) potential parameterized by Jiang [26] and the adaptive intermolecular reactive empirical bond order

(AIREBO) potential [27] are employed to describe the covalent interaction between the phosphorous (P) atoms in phosphorene and the carbon (C) atoms in graphene, respectively. The non-bonded vdW interactions among the different layers in the heterostructure are described by the Lennard-Jones (LJ) potential:

$$V(r_{ij}) = 4\varepsilon\left[(\sigma/r_{ij})^{12} - (\sigma/r_{ij})^{6}\right] \quad (1)$$

where r_{ij} is the distance between atoms i and j; ε and σ are the energy and distance constants, respectively. The parameters of the LJ potential used in the present MD simulations are listed in Table 1, which are obtained from the universal force field (UFF) model by Rappe *et al.* [28]. The cut-off distance of the LJ potential is chosen to be 15 Å.

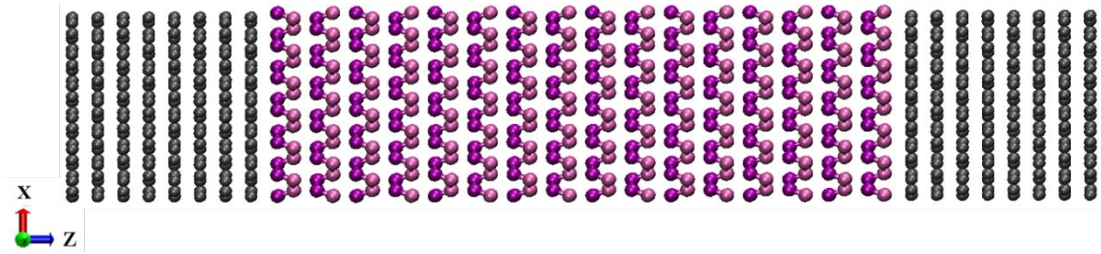

Figure 1. Simulation model of graphene/phosphorene/graphene (GE/BP/GE) heterostructure in which a 16-layer phosphorene is sandwiched in an 8-layer graphene at both ends.

Table 1. LJ potential parameters used in MD simulations.

Atom types	Energy constant ε (eV)	Distance constant σ (Å)
C-C	0.00455	3.431
P-P	0.0132	3.695
C-P	0.00775	3.563
H-P	0.00502	3.133

The thermal transport properties of the GE/BP/GE heterostructure are explored by using the reverse non-equilibrium molecular dynamics (NEMD) method based on Muller-Plathe's approach [29, 30]. The simulation model shown in Fig. 1 is divided into 32 slabs along the

cross-plane direction (z-direction). The simulation time step is 0.5 fs. The heat flux along the cross-plane direction is induced by continuously transferring energy from a "cold" slab that is located at the ends of the simulation model, to the "hot" slab which is located in the middle of the simulation model. Before applying the heat flux, the heterostructure is relaxed in two steps. First, the structure is relaxed in the NPT ensemble for 20000 time steps at each temperatures starting from the low temperature of 10 K, and increasing to 100 K, 200 K and room temperature of 300 K. Second, the system is switched to the NVE ensemble for 45 ps to conserve the energy. After that, the heat transfer between the heat source and heat sink slabs is induced by continuously exchanging the kinetic energies (every 200 time steps) between the hottest atom in the heat sink slab and the coldest atom in the heat source slab in the NVE ensemble. The heat flux J due to the kinetic energy exchange is then given by:

$$J = \frac{\sum_{N_t} \frac{1}{2}(m_h v_h^2 - m_c v_c^2)}{2At_t} \tag{2}$$

where N_t is the number of exchange, t_t summation time, A cross-section area that the heat energy passes through, subscripts h and c refer to the hottest and coldest atoms of which the kinetic energies are interchanged, respectively. The factor of 2 is due to the fact that the heat current propagated in two opposite directions from the hot region to the cold region. The system reaches a thermal steady state after exchanging energy between the heat source and heat sink slabs for 1 ns. A stable temperature profile can then be established between the heat source and heat sink slabs after the heat transfer reaches a steady state. A representative temperature profile of the heterostructure model is shown in Fig. 2 in which ΔT is the temperature drop at the graphene/phosphorene interface. This sudden temperature drop at the graphene/phosphorene interface should be attributed to their large different thermal properties and atomistic structures. The interfacial thermal conductance G is then calculated as:

$$G = J/\Delta T \tag{3}$$

By averaging the data collected over a period of 4 ns in the steady state, the final interfacial thermal conductance value is obtained. In the MD simulations, the temperature is obtained using the classical statistical mechanics equi-partition theorem, which is valid when the system temperature is higher than the Debye temperature of the material. To overcome this limitation, quantum corrections have been applied to the temperature and the thermal conductivity predicted by MD simulations [31]. However, recent study [32] found that employing quantum corrections to MD results above 200 K did not bring them to better agreement with the quantum predictions compared to the uncorrected MD results. In view of this fact, quantum corrections are neglected in the present work.

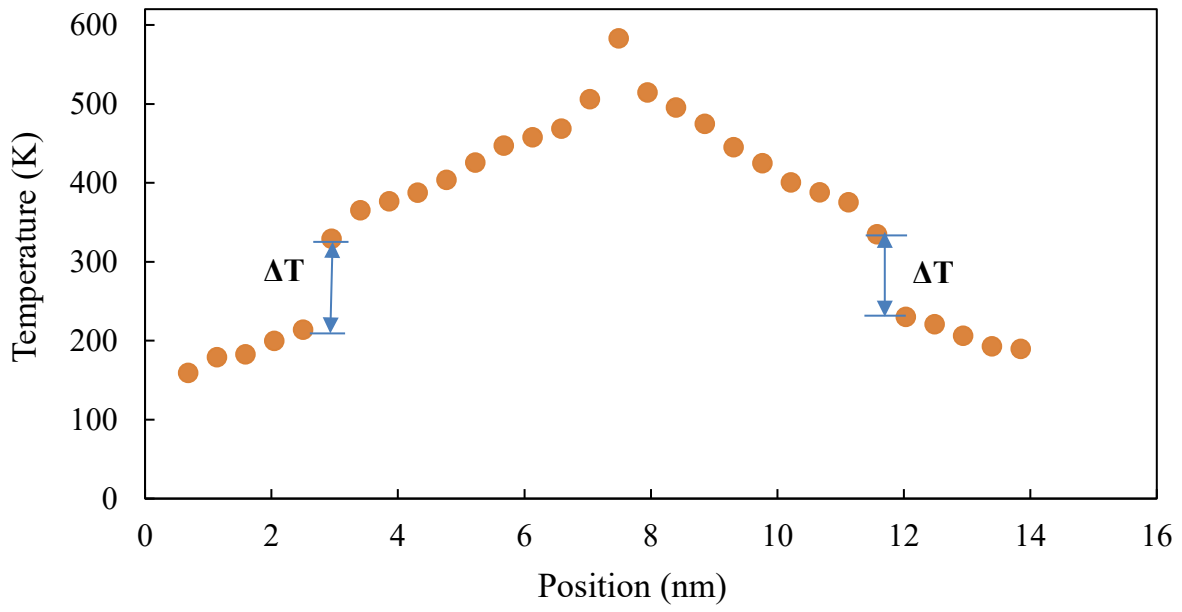

Figure 2. Typical temperature profile along the cross-plane direction in a GE/BP/GE heterostructure. A large temperature drop ΔT is observed at the interface between graphene and phosphorene.

It is well-known that the thermal properties of 2D nanomaterials, including graphene, phosphorene and MoS_2, are dependent on the size of the simulation model used as recognized by numerous studies in the literature [10, 33-35]. This aspect will not be studied here. Instead, in the present work, the model in Fig. 1 is simulated with the aim to explore how the

interfacial thermal conductance changes with defects, hydrogenation and mechanical strain. The effects of these factors are highlighted by normalizing the interfacial thermal conductance with that of the pristine case.

Thermal energy is the energy of atomic vibration in essence, which can be characterized by the vibration power spectrum or vibrational density of states (VDOS) in the frequency domain. VDOS can be determined by taking Fourier transform of the velocity auto-correlation function (VAF) of all the atoms as:

$$P(\omega) = \frac{1}{\sqrt{2\pi}} \int_0^{\tau} e^{i\omega t} \langle v(t)v(0) \rangle dt \quad (4)$$

where $P(\omega)$ is the total VDOS at frequency ω, the integration period $\tau = 0.2\ ns$, $\langle v(t)v(0) \rangle$ is the VAF and the brackets denote the ensemble average of all the atoms. For polarized VDOS, the VAF is calculated as $\langle v_x v_x + v_y v_y \rangle$ and $\langle v_z v_z \rangle$ for the in-plane and out-of-plane VDOS, respectively. The VDOS can be used to explain the underlying physics of the thermal transport property of the graphene/phosphorene heterostructure.

3. Results and discussion

3.1 Interfacial thermal conductance

Using Eqs. (2) and (3), the interfacial thermal conductance for the graphene/phosphorene heterostructure in Fig. 1 is calculated and listed in Table 2. It shows that the interfacial thermal conductance between two adjacent graphene layers is the highest (601.72 $MWm^{-2}K^{-1}$), followed by that between two adjacent phosphorene layers (259.54 $MWm^{-2}K^{-1}$). The thermal conductance between graphene and phosphorene interfaces (44.04 $MWm^{-2}K^{-1}$) is much lower than those of graphene/graphene and phosphorene/phosphorene interfaces. These results can be attributed to the different thermal properties of materials at the interfaces. The temperature profile in Fig. 2 shows that the temperature experiences a fast drop at the

graphene/phosphorene interface with ΔT = 105 K, which is induced by the distinctly different thermal transport properties of graphene and phosphorene. By contrast, the temperature profile at the interfaces of graphene/graphene and phosphorene/phosphorene show a continuous change without a sudden temperature drop. It is clearly shown that the interface thermal conductance depends heavily on the properties of the interfacial materials.

Table 2. Interfacial thermal conductance in GE/BP/GE heterostructure

Interface	Interfacial thermal conductance ($MWm^{-2}K^{-1}$)
Graphene/Graphene	601.72
Phosphorene/Phosphorene	259.54
Graphene/Phosphorene	44.04

The thermal conductivity in the cross-plane direction is also calculated using the Fourier law as: $\lambda = \frac{J}{(\partial T/\partial z)}$; for the graphene and phosphorene segments in the heterostructure, these values are 0.282 and 0.154 W/mK respectively. The cross-plane thermal conductivity of graphene is higher than that of phosphorene. It is well-known that graphene has a very high in-plane thermal conductivity of around 3000 W/mK due to the strongest sp^2 covalent bonds in the graphene structure [36] while the in-plane thermal conductivity of phosphorene is 43 W/mK in the zigzag direction and 9.89 W/mK in the armchair direction.[10] Compared to the in-plane thermal conductivity, the cross-plane thermal conductivities of graphene and phosphorene are much smaller due to the fact that the intra-layer interaction is governed by the weaker vdW interaction.

3.2 Effect of vacancy and hydrogenation

It is well-known that the thermal conductivity of nanomaterials can be effectively modulated by the presence of various defects in their structures. In the following, we study the effects of

vacancy defects and hydrogenations (carbon atoms in graphene are chemically bonded with hydrogen atoms) on the interfacial thermal conductance. Defect concentration is defined as the ratio of the number of defective atoms (vacancy or hydrogenation) over the total number of carbon atoms in a pristine graphene layer. Here, we focus on the interfacial thermal conductance at the interface of graphene and phosphorene; thus the defects were generated in the interfacial graphene layer adjacent to phosphorene only (i.e. defects are single-sided). In addition, we limit our investigation to the cases with low hydrogenation level (1-5%) since higher hydrogenation concentration (>10%) on a single-side of graphene leads to a distorted graphene structure.

Fig. 3 shows the change of the interfacial thermal conductance with increasing defect concentration. The interfacial thermal conductance of the defective heterostructure is normalized by that of the pristine interface (44.04 $MWm^{-2}K^{-1}$) in order to demonstrate the defect influence. Fig. 3 clearly shows that all the normalized interfacial thermal conductances are higher than 1.0, indicating that the presence of the vacancy defects or hydrogenation exerts positive effects on the interfacial thermal conductance. That is, the interfacial thermal conductance increases with increasing defect concentration. It is also found that hydrogenation is more effective than vacancy defects in improving the interfacial thermal conductance of the graphene/phosphorene heterostructure. For instance, at a defect concentration of 5%, the interfacial thermal conductance shows a 1.68-fold and 3.21-fold increase for vacancy defects and hydrogenation, respectively.

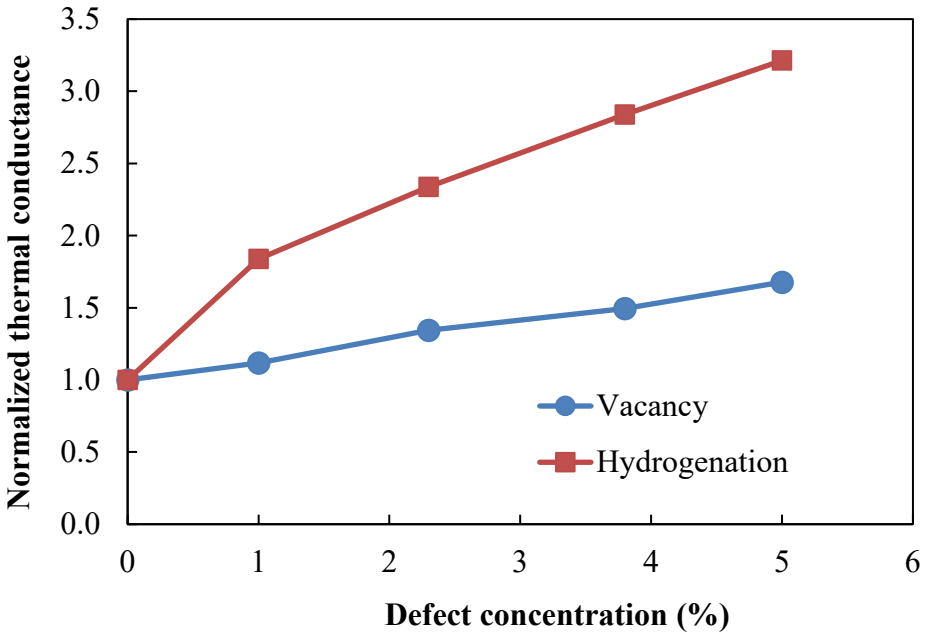

Figure 3. Interfacial thermal conductance as a function of defect concentration.

The enhancement in the interfacial thermal conductance induced by the defects can be explained by the elastic modulus mismatch and interfacial interaction strength. Recent MD simulations [37] and experimental work [38] confirmed that the interfacial thermal conductance can be enhanced by decreasing the modulus mismatch between filler and polymer matrix. Graphene and phosphorene are two distinct materials. When graphene is decorated with vacancy (carbon atom missing) and hydrogenation (transforming local C-C bonds in graphene from sp^2 to sp^3 hybridization), its Young's modulus (as well as thermal conductivity) decreases significantly and the elastic modulus mismatch between defective graphene and phosphorene is reduced accordingly. Hence, the interfacial thermal conductance between defective graphene and phosphorene increases and it increases with increasing defect concentration.

At the same density concentration, vacancy defects yield a larger reduction in Young's modulus of graphene than hydrogenation. From additional MD simulations conducted on monolayer graphene under uniaxial tension at a defect concentration of 5%, the Young's

moduli of vacancy defective and hydrogenated graphene are 0.598 and 0.967 TPa, respectively. Thus, the vacancy defect is more effective in reducing the elastic modulus mismatch between graphene and phosphorene. Nonetheless, as shown in Fig. 3 at the same defect content, the interfacial thermal conductance enhancement induced by vacancy defects is much lower than hydrogenation. This can be attributed to the effect of the interfacial interaction strength. The interfacial layers in the heterostructure interact with each other through the non-bonded vdW energy (C-P interaction for pristine and vacancy defective heterostructures). When interfacial graphene is functionalized by hydrogen, it gives rise to additional non-bonded P-H vdW interaction. The increased interfacial interaction strength (P-C and P-H) in the hydrogenated graphene/phosphorene heterostructure consequently leads to a higher interfacial thermal conductance**.** These findings are consistent with those given in Section 3.4 when the vdW interaction strength is increased by increasing the energy constant ε.

The superiority of hydrogenation over vacancy defects in improving the graphene/phosphorene interfacial thermal conductance can also be explained by the VDOS. Since we study the interfacial thermal conductance along the cross-plane (z) direction, the out-of-plane VDOS with the frequency range of 0-20 THz is plotted. Fig. 4 shows the out-of-plane VDOS at the interface for the phosphorene, graphene with 5% vacancies and graphene with 5% hydrogenation. As the modes of VDOS of graphene and phosphorene are in the same order, we compare their VDOS curves directly without normalizing by the area under the curve. The VDOS curves of phosphorene and graphene with hydrogenation (Fig. 4b) overlap better than phosphorene and graphene with vacancy defects (Fig. 4a), particularly, at frequency peaks near 10.5 and 11.9 THz. The better overlap in the VDOS curves means better heat conduction at the interface and thus higher interfacial thermal conductance.

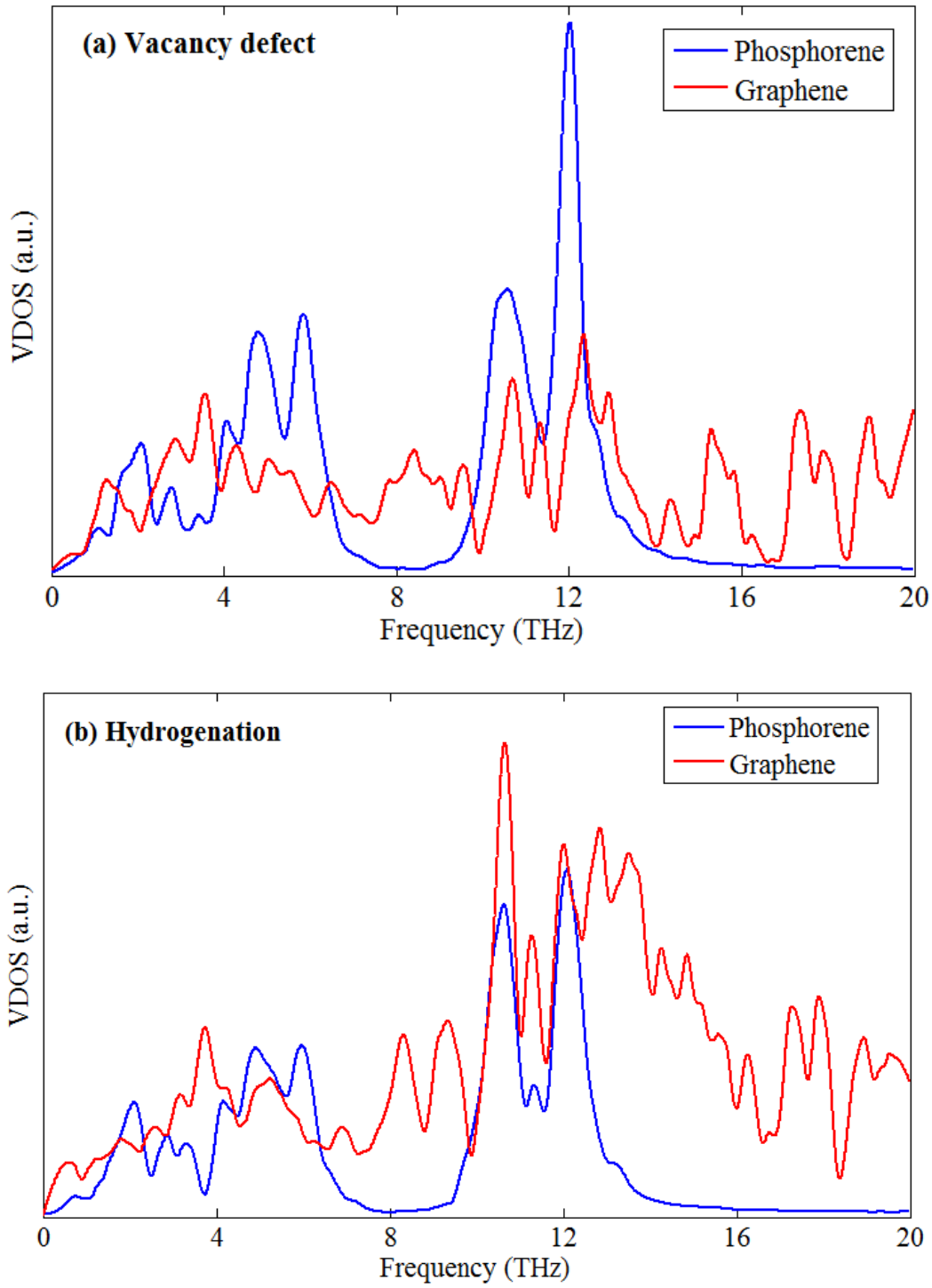

Figure 4. Out-of-plane VDOS of phosphorene and graphene at the interface in the graphene/phosphorene heterostructure for graphene with (a) 5% vacancies and (b) 5% hydrogenation.

When the vacancies are created in the phosphorene at the graphene/phosphorene interface, the interfacial thermal conductance of the heterostructure is lower than that with

vacancy created in graphene. For instance, at a defect concentration of 5%, the interfacial thermal conductance is 57.67 $MWm^{-2}K^{-1}$ for the defective-phosphorene/graphene interface, and 73.88 $MWm^{-2}K^{-1}$ for the defective-graphene/phosphorene interface. Both interfacial thermal conductance values are higher than that of the defect-free interface. These results imply that it is more effective to engineer vacancies in the stronger graphene for higher interfacial thermal conductance of the heterostructure, which is consistent with previous findings for polymer nanocomposites reinforced by stronger nano-fillers [37, 38].

3.3 Effect of cross-plane strain

External mechanical strain is proved to be an effective technique to manipulate the thermal properties of nanomaterials [39-46]. In the following, the effect of the tensile and compressive strains applied in the cross-plane direction (z-direction shown in Fig. 1) on the interfacial thermal conductance of the graphene/phosphorene heterostructures is investigated.

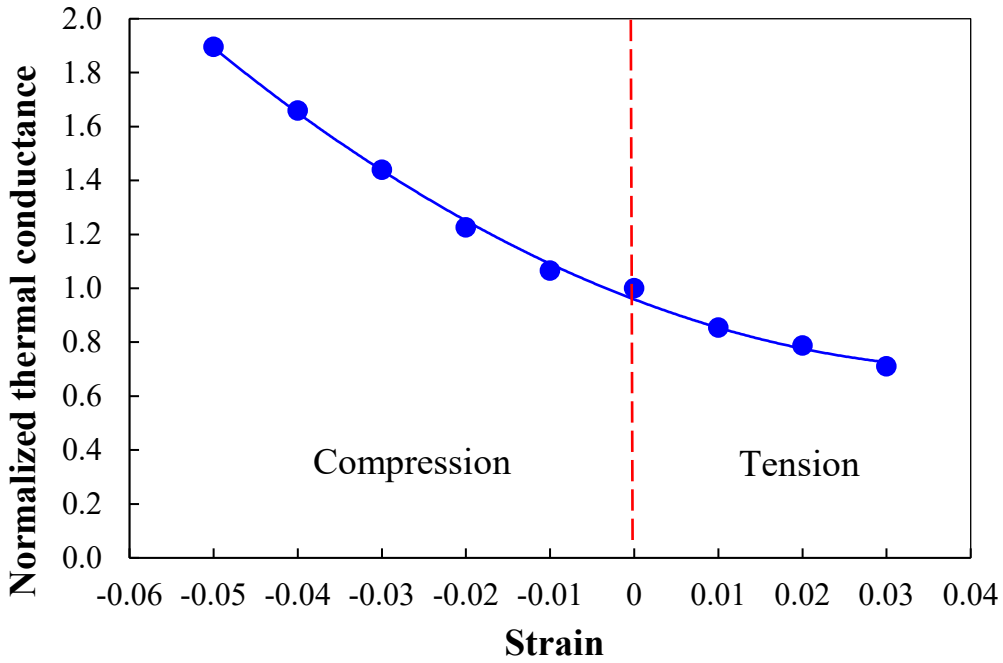

Figure 5. Normalized interfacial thermal conductance with respect to cross-plane strain.

Fig. 5 shows the variation of the graphene/phosphorene interfacial thermal conductance as a function of applied cross-plane strain. The interfacial thermal conductance is normalized by its value at zero strain. When the cross-plane strain changes from -0.05 (compression) to 0.03 (tension), the normalized interfacial thermal conductance decreases monotonically from 1.9 to 0.7, indicating that the cross-plane strain has a strong effect. When the heterostructure is under cross-plane compression/tension, the normalized interfacial thermal conductance is greater/smaller than 1, indicating that the applied cross-plane compressive/tensile strain enhances/reduces the interfacial thermal conductance. Specifically, at 0.05 cross-plane compressive strain the interfacial thermal conductance is increased by 90%, while at 0.03 cross-plane tensile strain the interfacial thermal conductance is decreased by 30%.

The cross-plane strains affect the interlayer interaction strength, and thus influence the thermal transport at the interface. Compressive cross-plane strain compacts the graphene/phosphorene heterostructure, reduces the interlayer distance and hence enhances the interlayer interaction at the interface. In turn, the stronger interlayer interaction facilitates heat transport, resulting in a higher interfacial thermal conductance. By contrast, tensile cross-plane strain increases the interlayer distance, weakens the interlayer interaction and consequently hinders the heat transport, leading to a lower interfacial thermal conductance.

The effect of the cross-plane strain on the interfacial thermal conductance is further supported by the VDOS results shown in Fig. 6. Apparently, compressive and tensile cross-plane strains induce phonon stiffening (increase) and softening (decrease) of the peak frequency, respectively. Phonon stiffening/softening increases/decreases the phonon group velocity, thus leading to an increase/decrease in the thermal conductance along the cross-plane direction [47].

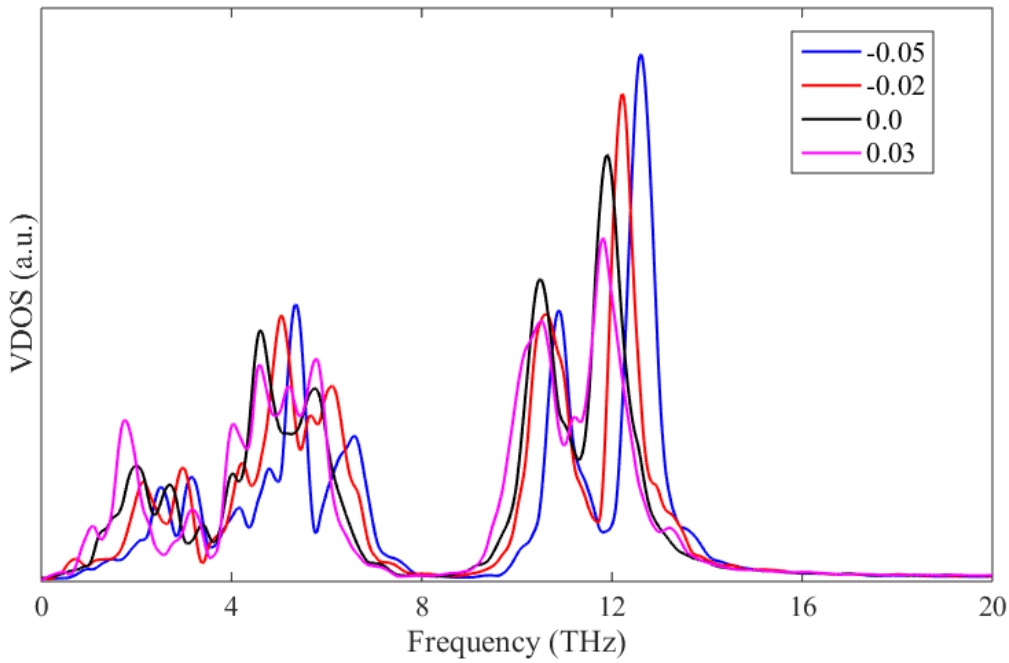

Figure 6. Out-of-plane VDOS of graphene/phosphorene heterostructure under different strains.

3.4 Effect of interlayer interaction strength

The non-bonded vdW interactions between different layers in the heterostructures are described by the LJ potential expressed in Eq. (1). To check the effect of the interlayer interaction strength on the interfacial thermal conductance, different interaction strength $\varepsilon = n\varepsilon_0$ is used in the MD simulations for the pristine heterostructure, where n is an integer and $\varepsilon_0 = 0.00775\, eV$ is the standard vdW interaction strength between graphene and phosphorene. The interfacial thermal conductance is normalized by the case having the standard ε_0. Increasing the interlayer interaction strength by manually increasing $\varepsilon = n\varepsilon_0$ where n=2-4, the interfacial thermal conductance increases nearly linearly as shown in Fig. 7. From the VDOS in Fig. 8, it is clearly displayed that a higher interlayer interaction strength leads to a better match of the VDOS curves of graphene and phosphorene, thus facilitating heat transport across the graphene/phosphorene interface. As a consequence, the interfacial thermal conductance is considerably increased.

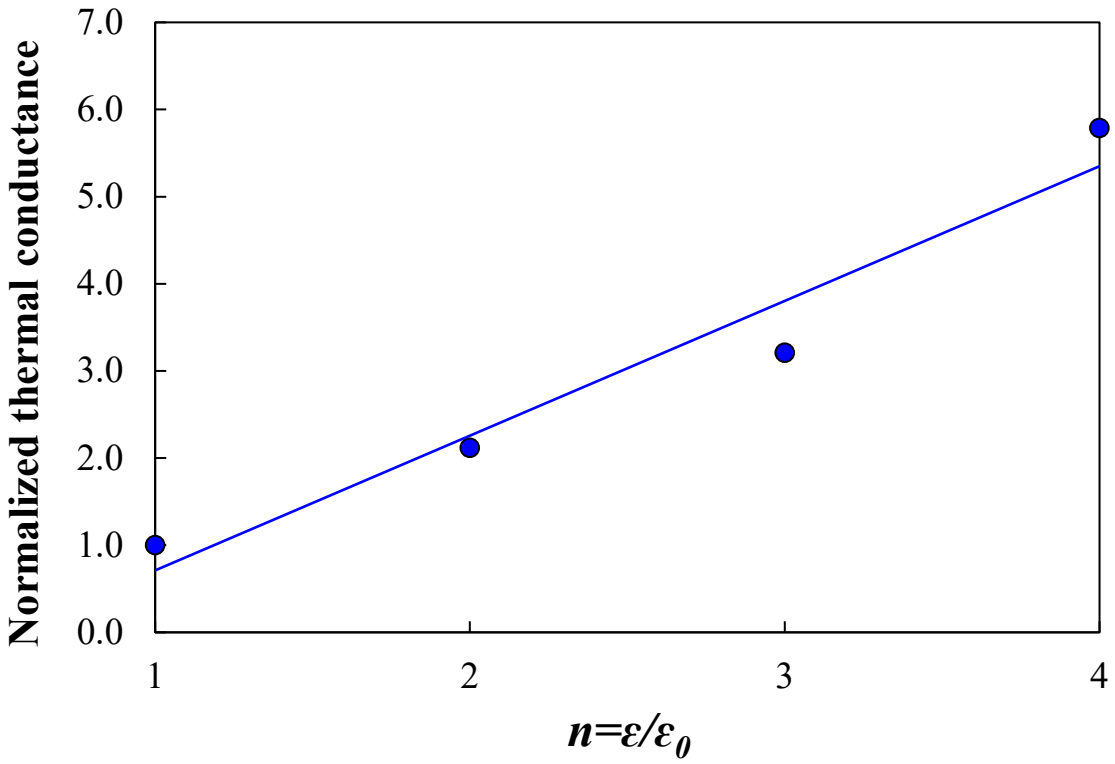

Figure 7. Normalized interfacial thermal conductance as a function of interlayer interaction strength $n = \varepsilon/\varepsilon_0$.

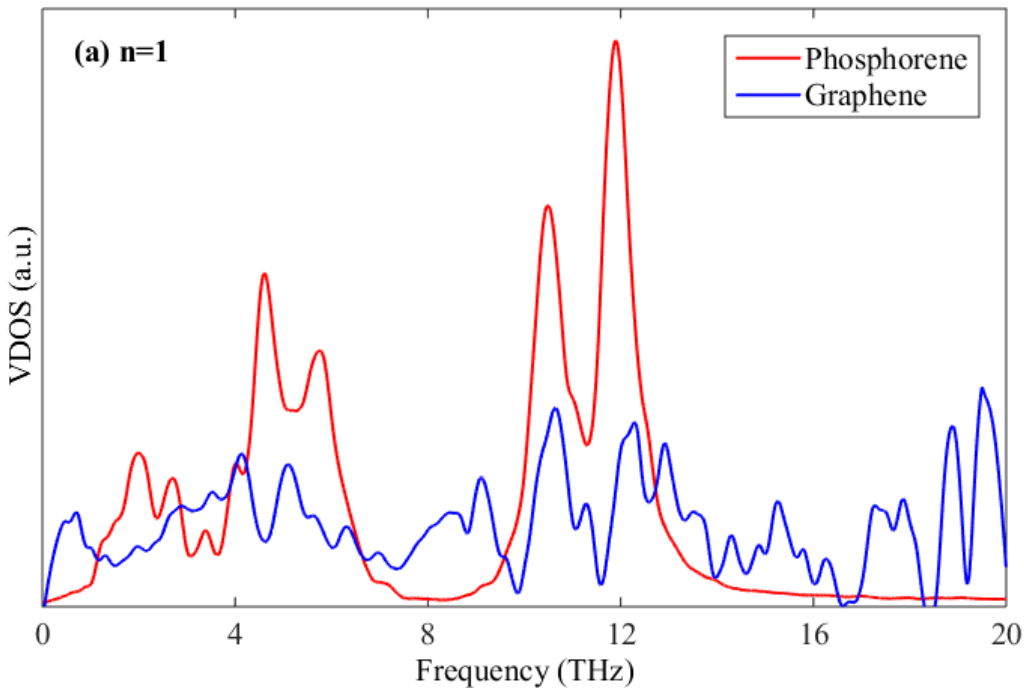

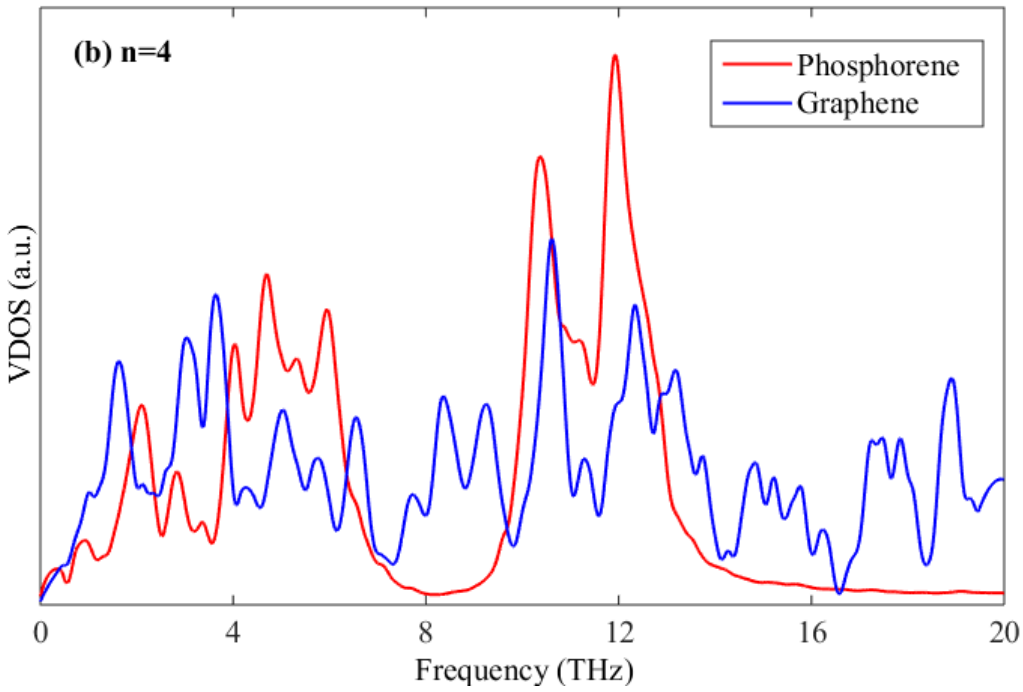

Figure 8. Out-of-plane VDOS of graphene/phosphorene heterostructure with different interfacial interaction strength. (a) Standard strength $\varepsilon = \varepsilon_0$ and (b) enhanced strength $= 4\varepsilon_0$.

4. Conclusions

Extensive MD simulations have been performed to investigate the thermal transport in graphene/phosphorene heterostructures along the cross-plane direction. Based on the simulation results, the interfacial thermal conductance at the graphene/phosphorene interface can be effectively controlled by vacancy defects, hydrogenation and external cross-plane strain. At the largest defect concentration of 5%, the hydrogenation and vacancy defects created in the interfacial graphene layer can bring 3.21-fold and 1.68-fold increase in interfacial thermal conductance. This defect-induced enhancement of the interfacial thermal conductance is attributed to the decreased elastic modulus mismatch and the increased interlayer interaction strength between graphene and phosphorene. The interfacial thermal conductance can also be manipulated by applying a cross-plane strain to the graphene/phosphorene heterostructures. A cross-plane compressive strain of 0.05 can

increase the interfacial thermal conductance by 90%, whereas a cross-plane tensile strain of 0.03 can reduce the interfacial thermal conductance by 30%. The present work provides important guidelines for manipulating and controlling thermal transport in graphene/phosphorene based-nanodevices.

Acknowledgements

Y.Y. Zhang is grateful for the computational support provided by Intersect Australia Ltd and 2015 Academic Development Program in Western Sydney University, Australia. S. K. Lai is grateful for the financial support provided by the Start-up Fund Project of The Hong Kong Polytechnic University (Project No. 1-ZE4V).

References

[1] Novoselov K S, Geim A K, Morozov S V, Jiang D, Zhang Y, Dubonos S V, Grigorieva I V and Firsov A A 2004 Electric field effect in atomically thin carbon films *Science* **306** 666-9

[2] Soldano C, Mahmood A and Dujardin E 2010 Production, properties and potential of graphene *Carbon* **48** 2127-50

[3] Castro Neto A H, Guinea F, Peres N M R, Novoselov K S and Geim A K 2009 The electronic properties of graphene *Rev Mod. Phys.* **81** 109-62

[4] Liu H, Neal A T, Zhu Z, Luo Z, Xu X, Tomanek D and Ye P D 2014 Phosphorene: An Unexplored 2D Semiconductor with a high hole mobility *ACS Nano* **8** 4033-41

[5] Brent J R, Savjani N, Lewis E A, Haigh S J, Lewis D J and O'Brien P 2014 Production of few-layer phosphorene by liquid exfoliation of black phosphorus *Chem. Commun.* **50** 13338-41

[6] Liu H, Du Y C, Deng Y X and Ye P D 2015 Semiconducting black phosphorus: synthesis, transport properties and electronic applications *Chem. Soc. Rev.* **44** 2732-43

[7] Li L, Yu Y, Ye G J, Ge Q, Ou X, Wu H, Feng D, Chen X H and Zhang Y 2014 Black phosphorus field-effect transistors *Nat. Nanotechnol.* **9** 372-7

[8] Xia F, Wang H and Jia Y 2014 Rediscovering black phosphorus as an anisotropic layered material for optoelectronics and electronics *Nat. Commun.* **5** 4458

[9] Hong Y, Zhang J, Huang X and Zeng X C 2015 Thermal conductivity of a two-dimensional phosphorene sheet: a comparative study with graphene *Nanoscale* **7** 18716-24

[10] Zhang Y Y, Pei Q X, Jiang J W, Wei N and Zhang Y W 2016 Thermal conductivities of single- and multi-layer phosphorene: a molecular dynamics study *Nanoscale* **8** 483-91

[11] Fei R, Faghaninia A, Soklaski R, Yan J-A, Lo C and Yang L 2014 Enhanced Thermoelectric Efficiency via Orthogonal Electrical and Thermal Conductances in Phosphorene *Nano Lett.* **14** 6393-9

[12] Geim A K and Grigorieva I V 2013 Van der Waals heterostructures *Nature* **499** 419-25

[13] Roy K, Padmanabhan M, Goswami S, Sai T P, Ramalingam G, Raghavan S and Ghosh A 2013 Graphene-MoS2 hybrid structures for multifunctional photoresponsive memory devices *Nat. Nanotechnol.* **8** 826-30

[14] Antonova I V 2016 Vertical heterostructures based on graphene and other 2D materials *Semiconductors* **50** 66-82

[15] Lotsch B V 2015 Vertical 2D Heterostructures *Annu. Rev. Mater Res.* **45** 85-109

[16] Liu B, Baimova J A, Reddy C D, Law A, Dmitriev S V, Wu H and Zhou K 2014 Interfacial Thermal Conductance of a Silicene/Graphene Bilayer Heterostructure and the Effect of Hydrogenation *ACS Appl. Mater. Interfaces* **6** 18180-8

[17] Liu B, Meng F, Reddy C D, Baimova J A, Srikanth N, Dmitriev S V and Zhou K 2015 Thermal transport in a graphene-MoS2 bilayer heterostructure: a molecular dynamics study *RSC Adv.* **5** 29193-200

[18] Qian X, Wang Y, Li W, Lu J and Li J 2015 Modelling of stacked 2D materials and devices *2D Mater.* **2** 032003

[19] Zhang Z, Xie Y, Peng Q and Chen Y 2015 Thermal transport in MoS2/Graphene hybrid nanosheets *Nanotechnology* **26** 375402

[20] Kang J, Horzum S and Peeters F M 2015 Heterostructures of graphene and nitrogenated holey graphene: Moire pattern and Dirac ring *Phys. Rev. B* **92** 195419

[21] Padilha J E, Fazzio A and da Silva A J R 2015 van der Waals Heterostructure of Phosphorene and Graphene: Tuning the Schottky Barrier and Doping by Electrostatic Gating *Phys. Rev. Lett.* **114** 066803

[22] Chen X, Wu Y, Wu Z, Han Y, Xu S, Wang L, Ye W, Han T, He Y, Cai Y and Wang N 2015 High-quality sandwiched black phosphorus heterostructure and its quantum oscillations *Nat. Commun.* **6** 7315

[23] Vallabhaneni A K, Qiu B, Hu J N, Chen Y P, Roy A K and Ruan X L 2013 Interfacial thermal conductance limit and thermal rectification across vertical carbon nanotube/graphene nanoribbon-silicon interfaces *J Appl. Phys.* **113** 064311

[24] Chen X K, Xie Z X, Zhou W X and Chen K Q 2016 The thermal conductivity in hybridised graphene and boron nitride nanoribbons modulated with strain *J. Phys. D: Appl. Phys.* **49** 115301

[25] Plimpton S 1995 Fast parallel algorithms for short-range molecular dynamics *J. Comput. Phys.* **117** 1-19

[26] Jiang J W 2015 Parametrization of Stillinger-Weber potential based on valence force field model: application to single-layer MoS2 and black phosphorus *Nanotechnology* **26** 315706

[27] Stuart S J, Tutein A B and Harrison J A 2000 A reactive potential for hydrocarbons with intermolecular interactions *J. Chem. Phys.* **112** 6472

[28] Rappé A K, Casewit C J, Colwell K S, Goddard Iii W A and Skiff W M 1992 UFF, a full periodic table force field for molecular mechanics and molecular dynamics simulations *J. Am. Chem. Soc.* **114** 10024-35

[29] MullerPlathe F 1997 A simple nonequilibrium molecular dynamics method for calculating the thermal conductivity *J. Chem. Phys.* **106** 6082-5

[30] Schelling P K, Phillpot S R and Keblinski P 2002 Comparison of atomic-level simulation methods for computing thermal conductivity *Phys. Rev. B* **65** 144306

[31] Wang C Z, Chan C T and Ho K M 1990 Tight-Binding molecular-dynamics study of phonon anharmonic effects in silicon and diamond *Phys. Rev. B* **42** 11276-83

[32] Turney J E, McGaughey A J H and Amon C H 2009 Assessing the applicability of quantum corrections to classical thermal conductivity predictions *Phys. Rev. B* **79** 224305

[33] Bagri A, Kim S P, Ruoff R S and Shenoy V B 2011 Thermal transport across twin grain boundaries in polycrystalline graphene from nonequilibrium molecular dynamics dimulations *Nano Lett.* **11** 3917-21

[34] Ding Z W, Jiang J W, Pei Q X and Zhang Y W 2015 In-plane and cross-plane thermal conductivities of molybdenum disulfide *Nanotechnology* **26** 065703

[35] Pei Q X, Zhang Y W, Sha Z D and Shenoy V B 2013 Tuning the thermal conductivity of silicene with tensile strain and isotopic doping: A molecular dynamics study *J. Appl. Phys.* **114** 033526

[36] Balandin A A, Ghosh S, Bao W, Calizo I, Teweldebrhan D, Miao F and Lau C N 2008 Superior thermal conductivity of single-layer graphene *Nano Lett.* **8** 902-7

[37] Hu M, Shenogin S and Keblinski P 2007 Molecular dynamics simulation of interfacial thermal conductance between silicon and amorphous polyethylene *Appl. Phys. Lett.* **91** 241910

[38] Cui W, Du F, Zhao J, Zhang W, Yang Y, Xie X and Mai Y W 2011 Improving thermal conductivity while retaining high electrical resistivity of epoxy composites by incorporating silica-coated multi-walled carbon nanotubes *Carbon* **49** 495-500

[39] Han X Y, Stewart H M, Shevlin S A, Catlow C R A and Guo Z X 2014 Strain and orientation modulated bandgaps and effective masses of phosphorene nanoribbons *Nano Lett.* **14** 4607-14

[40] Lindsay L, Li W, Carrete J, Mingo N, Broido D A and Reinecke T L 2014 Phonon thermal transport in strained and unstrained graphene from first principles *Phys. Rev. B* **89** 155426

[41] Bhowmick S and Shenoy V B 2006 Effect of strain on the thermal conductivity of solids *J. Chem. Phys.* **125** 164513

[42] Guo Z X, Zhang D and Gong X G 2009 Thermal conductivity of graphene nanoribbons *Appl. Phys. Lett.* **95** 163103

[43] Wei N, Xu L Q, Wang H Q and Zheng J C 2011 Strain engineering of thermal conductivity in graphene sheets and nanoribbons: a demonstration of magic flexibility *Nanotechnology* **22** 105705

[44] Zhang G and Zhang Y W 2015 Strain effects on thermoelectric properties of two-dimensional materials *Mech. Mater.* **91** 382-98

[45] Li X B, Maute K, Dunn M L and Yang R G 2010 Strain effects on the thermal conductivity of nanostructures *Phys. Rev. B* **81** 245318

[46] Zhan H F, Zhang G, Bell J M and Gu Y T 2014 Thermal conductivity of configurable two-dimensional carbon nanotube architecture and strain modulation *Appl. Phys. Lett.* **105** 153105

[47] Chen J, Walther J H and Koumoutsakos P 2014 Strain Engineering of Kapitza Resistance in Few-Layer Graphene *Nano Lett.* **14** 819-25